AFRL-ML-WP-TR-2000-4060

SPLINE VARIATIONAL THEORY FOR COMPOSITE BOLTED JOINTS

E. V. IARVE AND R. Y. KIM

UNIVERSITY OF DAYTON RESEARCH INSTITUTE
300 COLLEGE PARK AVENUE
DAYTON, OHIO 45469-0168

APRIL 2000

INTERIM REPORT FOR 09/15/98-09/14/1999

PUBLIC RELEASE; DISTRIBUTION UNLIMITED

MATERIALS AND MANUFACTURING DIRECTORATE
AIR FORCE RESEARCH LABORATORY
AIR FORCE MATERIEL COMMAND
WRIGHT-PATTERSON AIR FORCE BASE, OH 45433-7734

REPORT DOCUMENTATION PAGE

1. REPORT DATE (DD-MM-YYYY) 01-04-2000	2. REPORT TYPE final	3. DATES COVERED (FROM - TO) 15-09-1998 to 14-09-1999

4. TITLE AND SUBTITLE Spline Variational Theory for Composite Bolted Joints Unclassified	5a. CONTRACT NUMBER
	5b. GRANT NUMBER
	5c. PROGRAM ELEMENT NUMBER

6. AUTHOR(S) Iarve, E. V. ; Kim, R. Y. ;	5d. PROJECT NUMBER
	5e. TASK NUMBER
	5f. WORK UNIT NUMBER

7. PERFORMING ORGANIZATION NAME AND ADDRESS University of Dayton Research Institute 300 College Park Avenue Dayton , OH 45469-0168	8. PERFORMING ORGANIZATION REPORT NUMBER UDR-TR-1999-00095

9. SPONSORING/MONITORING AGENCY NAME AND ADDRESS Materials and Manufacturing Directorate Air Force Research Laboratory Air Force Materiel Command Wright-Patterson AFB , OH 45433-7334	10. SPONSOR/MONITOR'S ACRONYM(S) AFRL/MLBC
	11. SPONSOR/MONITOR'S REPORT NUMBER(S) AFRL-ML-WP-TR-2000-4060

12. DISTRIBUTION/AVAILABILITY STATEMENT
A
PUBLIC RELEASE

Materials and Manufacturing Directorate
Air Force Research Laboratory
Air Force Materiel Command
Wright-Patterson AFB , OH 45433-7334

13. SUPPLEMENTARY NOTES

14. ABSTRACT

Three dimensional failure initiation and progression modeling and the experimental work required to verify the analysis methods were conducted.

15. SUBJECT TERMS

composite; bolted joint; three-dimensional stress analysis; damage initiation prediction; stacking sequence effect; damage progression; acoustic emission; incremental loading; x-radiography

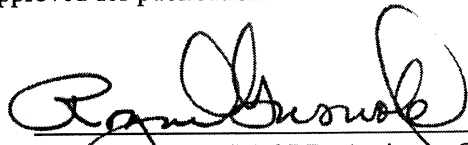| 16. SECURITY CLASSIFICATION OF:			17. LIMITATION OF ABSTRACT	18. NUMBER OF PAGES	19a. NAME OF RESPONSIBLE PERSON
			Public Release	48	Fenster, Lynn lfenster@dtic.mil
a. REPORT Unclassified	**b. ABSTRACT** Unclassified	**c. THIS PAGE** Unclassified			**19b. TELEPHONE NUMBER** **International Area Code** **Area Code Telephone Number** 703 767-9007 DSN 427-9007

NOTICE

Using Government drawings, specifications, or other data included in this document for any purpose other than Government procurement does not in any way obligate the U.S. Government. The fact that the Government formulated or supplied the drawings, specifications, or other data does not license the holder or any other person or corporation; or convey any rights or permission to manufacture, use, or sell any patented invention that may relate to them.

This report is releasable to the National Technical Information Service (NTIS). At NTIS, it will be available to the general public, including foreign nations.

This technical report has been reviewed and is approved for publication.

L. SCOTT THEIBERT, Chief
Structural Materials Branch
Nonmetallic Materials Division

ROGER D. GRISWOLD, Assistant Chief
Nonmetallic Materials Division
Materials and Manufacturing Directorate

Do not return copies of this report unless contractual obligations or notice on a specific document requires its return.

REPORT DOCUMENTATION PAGE		*Form Approved* *OMB No. 074-0188*

Public reporting burden for this collection of information is estimated to average 1 hour per response, including the time for reviewing instructions, searching existing data sources, gathering and maintaining the data needed, and completing and reviewing this collection of information. Send comments regarding this burden estimate or any other aspect of this collection of information, including suggestions for reducing this burden to Washington Headquarters Services, Directorate for Information Operations and Reports, 1215 Jefferson Davis Highway, Suite 1204, Arlington, VA 22202-4302, and to the Office of Management and Budget, Paperwork Reduction Project (0704-0188), Washington, DC 20503

1. AGENCY USE ONLY (Leave blank)	2. REPORT DATE April 2000	3. REPORT TYPE AND DATES COVERED Final report for 09/15/98 – 09/14/99	

4. TITLE AND SUBTITLE
SPLINE VARIATIONAL THEORY FOR COMPOSITE BOLTED JOINTS

6. AUTHOR(S)

E. V. IARVE AND R. Y. KIM

5. FUNDING NUMBERS
C: F33615-95-D-5029
PE: 61102
PR: 4347
TA: 34
WU: 10

7. PERFORMING ORGANIZATION NAME(S) AND ADDRESS(ES)

UNIVERSITY OF DAYTON RESEARCH INSTITUTE
300 COLLEGE PARK AVENUE
DAYTON, OH 45469-0168

8. PERFORMING ORGANIZATION REPORT NUMBER

UDR-TR-1999-00095

9. SPONSORING / MONITORING AGENCY NAME(S) AND ADDRESS(ES)

Materials and Manufacturing Directorate
Air Force Research Laboratory
Air Force Materiel Command
Wright-Patterson AFB OH 45433-7334
POC: L. SCOTT THEIBERT, AFRL/MLBC, 937-255-9070

10. SPONSORING / MONITORING AGENCY REPORT NUMBER

AFRL-ML-WP-TR-2000-4060

11. SUPPLEMENTARY NOTES

12a. DISTRIBUTION / AVAILABILITY STATEMENT

APPROVED FOR PUBLIC RELEASE; DISTRIBUTION UNLIMITED

12b. DISTRIBUTION CODE

13. ABSTRACT *(Maximum 200 Words)*
Three dimensional failure initiation and progression modeling and the experimental work required to verify the analysis methods were conducted. Damage initiation and progression in the unidirectional and quasi-isotropic laminates was modeled based on the property degradation methodology. Reissner-Hellinger variational principle was applied to rigorously represent the degraded material properties in order to model the discrete damage at the hole edge. A recursive algorithm based on damage increment concept was developed to perform the damage evolution modeling. Both mechanical loading and residual stresses were taken into account. Conventional finite-element formulation based on linear displacement approximation was used. The analysis uncovered severe mesh type dependence of the damage evolution modeling based on conventional finite-element approximation. The results showed that only a specific class of finite-element meshes allows describing the stress relaxation in the fiber direction in unidirectional laminates with holes occurring due to matrix splitting under uniaxial tension. An experimental investigation has been conducted on the initiation and growth of damage in close proximity to the open hole for the [±30/902]S and [02/902]S laminates under incremental tension loading. For both laminates the analytical predictions of strain calculated by spline variational theory and by elasticity showed good agreement with experimentally measured results. The development of damage observed by x-radiography was correlated with the stress-strain behavior.

14. SUBJECT TERMS
composite, bolted joint, three-dimensional stress analysis, damage Initiation prediction, stacking sequence effect, damage progression, acoustic emission, incremental loading, x-radiography

15. NUMBER OF PAGES
61

16. PRICE CODE

17. SECURITY CLASSIFICATION OF REPORT UNCLASSIFIED	18. SECURITY CLASSIFICATION OF THIS PAGE UNCLASSIFIED	19. SECURITY CLASSIFICATION OF ABSTRACT UNCLASSIFIED	20. LIMITATION OF ABSTRACT SAR

CONTENTS

FIGURES

FIGURES (Concluded)

TABLES

FOREWORD

This report was prepared by the University of Dayton Research Institute under Air Force Contract No. F33615-95-D-5029, Delivery Order No. 0004. The work was administered under the direction of the Nonmetallic Materials Division, Materials and Manufacturing Directorate, Air Force Research Laboratory, Air Force Materiel Command, with Dr. James R. McCoy (AFRL/MLBC) as Project Engineer.

This report was submitted in November 1999 and covers work conducted from 15 September 1998 through 14 September 1999.

EXECUTIVE SUMMARY

Three-dimensional failure initiation and progression modeling and the experimental work required to verify the analysis methods are reported below. The stacking sequence effect on pin bearing strength was examined by three-dimensional modeling. A displacement spline approximation method was used to perform the stress analysis. The laminate and the fastener were assumed to be linear elastic. Processing residual stresses were included in the analysis. The contact region and stress were unknown *a priori* and resulted from the solution. A nonuniform contact region through the thickness was allowed. Undamaged thermoelastic moduli were employed in the model. The stacking sequence effect on bearing strength was investigated by comparing stress distributions in two quasi-isotropic laminates of $[0_2/90_2/45_2/-45_2]_s$ and $[0_2/45_2/90_2/-45_2]_s$ stacking sequence. Stress magnitudes were displayed relative to ply strength properties. It was observed that all stress components, including the in-plane stresses, were affected by the stacking sequence. In the vicinity of the bearing plane, very high transverse shear stresses were found. Using a point stress failure criterion, a prediction of failure onset was performed. The predicted failure initiation load for the $[0_2/90_2/45_2/-45_2]_s$ stacking sequence was approximately 40 percent higher than the predicted failure initiation load for the $[0_2/45_2/90_2/-45_2]_s$ stacking sequence.

Damage initiation and progression in the unidirectional and quasi-isotropic laminates was modeled based on the property degradation methodology. The Reissner-Hellinger variational principle was applied to rigorously represent the degraded material properties in order to describe discrete damage at the hole edge. A recursive algorithm based on the damage increment concept was developed to perform the damage evolution modeling. Both mechanical loading and residual stresses were taken into account. The maximum stress

1

failure criterion was implemented and used to select the elements where the properties were degraded. Conventional finite element formulation based on linear displacement approximation was used. The analysis uncovered severe mesh-type dependence of the damage evolution modeling based on conventional finite element approximation. The results showed that only a specific class of finite element meshes allows one to describe the stress relaxation in the fiber direction in unidirectional laminates with holes occurring due to matrix splitting under uniaxial tension. Further research will be conducted to employ unconventional methods such as spline mesh overlays and spline basis enrichment approach to discrete damage modeling in laminates with holes.

An experimental investigation has been conducted on the initiation and growth of damage in close proximity to open hole for the $[\pm30/90_2]_S$ and $[0_2/90_2]_S$ laminates under incremental tension loading. For both laminates, the analytical predictions of strain calculated by spline variational theory and by elasticity showed good agreement with experimentally measured results. The development of damage observed by x-radiography was correlated with the stress-strain behavior. As damage developed for both laminates, stress concentration decreased, and the net stress at failure was nearly identical to the static strength of the respective unnotched coupon. However, for the first-ply failure, the net stress onset is related through a reduced stress concentration factor. This experimental work continues on the $[\pm45/90/0]_S$ and $[45/0/-45/90]_S$ laminates.

1. THREE-DIMENSIONAL STRESS ANALYSIS AND FAILURE PREDICTION IN FILLED-HOLE LAMINATES

Bolted joining remains a primary joining method of load carrying composite structural elements in the modern aerospace industry. Significant attention in the literature has been given to practically all aspects of composite bolted joining, both in the analysis and experimental fields as described in a recent survey *[1]*. The need for a composite bolted joint design tool led to development of several composite bolted joint failure prediction programs, reviewed by Snyder et al. *[2]*, and utilized in the industry. The common mechanical foundation for all of these tools reviewed is lamination theory combined with average or point stress failure criterion to predict final strength. A different failure prediction methodology, based on fracture mechanics, was developed in *[3,4]* and is based on pseudo-crack propagation in the radial direction from the hole edge. Energy release rates for these cracks are obtained by utilizing the rule of mixtures and the number of plies of each orientation – 0, ±45, and 90 – in the laminate. In all of the above methods, the fastener-plate contact stress is assumed to vary as a cosine function over half the hole circumference with an amplitude of -4/π times the nominal bearing stress. The advantage of these largely empirical approaches is that a broad spectrum of problems can be solved without significant computer resources. The disadvantage is the need for an extensive test database that is required for each new material system utilized. To develop new tools for composite bolted joint design and strength prediction based on measured ply properties, an in-depth understanding of the bearing failure mechanisms is important. Recent experimental works *[5-7]* dealing with graphite-epoxy laminates provide detailed investigations of the bearing failure process and show similar results. The specimens subjected to bearing loading were

x-rayed and sectioned at different load levels lower or equal to the failure load. Microscopic studies of the bearing plane sections showed that bearing failure consists of a damage accumulation process initiated in the interior of the laminate at the hole edge. It consists of 45° transverse shear cracks propagating to the outer surfaces from the hole edge. According to *[6,7]* in the case of a pin-loaded hole, these cracks reach the outer surfaces at approximately a quarter of the laminate thickness away from the hole edge, resulting in final failure. In all cases massive delamination was observed on the interior interfaces prior to failure. In the presence of clamping forces *[8]*, the damage mechanism does not seem to change. The failure load significantly increases because the final failure does not occur until the damage accumulation region reaches the outer washer diameter, provided that the washer can carry the increasing plate expansion force. As concluded in *[5,6]*, the bearing failure is a substantially three-dimensional process involving delamination and transverse shear; although in the sequel of works *[7,8]*, the authors proposed a two-dimensional bearing strength prediction model, which was shown to provide good correlation with experimentally-measured bearing strength. This model is based on nonlinear finite element simulation with gradual property degradation algorithms.

Lamination theory, however, cannot account for stacking sequence effects on bearing strength. Hamada et al. *[5]* tested four symmetric laminates stacked with sequences of 0_2, 45_2, -45_2, and 90_2 ply groups. The material used was T300/2500. The bearing strength results obtained in *[5]* are summarized in Table 1, and the specimen geometry used throughout this research is shown in Figure 1. An approximately 13 percent difference was observed for specimens C and N, corresponding to stacking sequences $[0_2/90_2/45_2/-45_2]_s$ and $[0_2/45_2/90_2/-45_2]_s$, respectively. These specimens differ by an apparently minor alteration in

Table 1
Experimental Bearing Failure Stresses Obtained from [1]

Specimen Identification and Stacking Sequence	Bearing Stress (MPa)
N -- $[0_2/+45_2/90_2/-45_2]_s$	318
A -- $[0_2/+45_2/-45_2/90_2]_s$	333
B -- $[-45_2/0_2/+45_2/90_2]_s$	338
C -- $[0_2/90_2/+45_2/-45_2]_s$	360

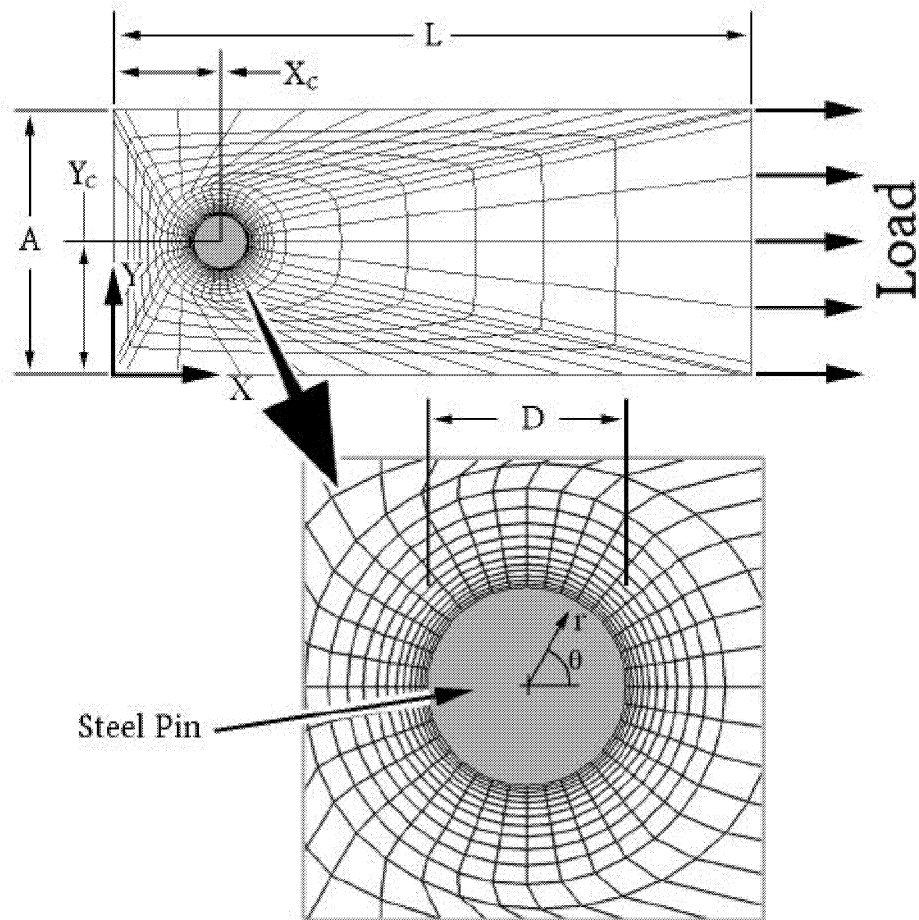**Figure 1.** Specimen Geometry. L=72 mm, A=30 mm, D=6 mm, Xc= 12 mm, Yc=15 mm, and ply thickness ~0.25 mm.

stacking sequence only. The only difference is in exchanging the 90° and 45° plies while retaining the position of the 0° plies on the outside and -45° plies at the midsurface. The purpose of the present work is to perform three-dimensional stress analysis to explain the effect that such a small change of the stacking sequence can have on laminate pin bearing strength. Damage related stress redistribution was not considered in this research.

A previously developed fully three-dimensional stress analysis procedure *[9]* was used to examine the stress distributions occurring under bearing loading. The procedure is based on a cubic spline approximation of displacements along with a curvilinear transformation technique also based on the spline approximation. Due to the highly nonuniform stress-strain field through the thickness of the laminate, the contact zone becomes nonuniform through the thickness. An automated algorithm was developed for contact zone definition. Verification of the results of the interlaminar stress prediction was accomplished by comparison with the asymptotic solution.

1.1   Problem Definition

Consider a rectangular orthotropic plate containing a circular hole having a diameter D, as shown in Figure 1. The plate consists of N plies of total thickness H in the z-direction, has a length L in the x-direction and width A in the y-direction. A circular isotropic elastic fastener of diameter d is situated at the center of the hole. The length of the fastener in the z-direction is equal to the plate thickness H. We will consider the bearing loading case when the load is applied via displacement boundary conditions at x=L, while all other boundaries were kept free:

$$u_x(L,y,z) = u_L, \quad u_y(L,y,z) = u_z(L,y,z) = 0,$$
$$\sigma_{xx}(0,y,z) = \sigma_{xy}(0,y,z) = \sigma_{xz}(0,y,z) = 0 \tag{1}$$

A cylindrical coordinate system is defined originating from the center of the hole:

$$x = r\cos\theta + x_c, \, y = r\sin\theta + y_c, \, z = z,$$ (2)

where x_c and y_c are the coordinates of the center of the hole. The fastener displacements will be denoted as v_r, v_θ, and v_z. The in-plane motion of the fastener is fixed at two points located at the center of the top and bottom fastener surfaces $z=0$ and $z=H$, and the z displacement is fixed at the mid-surface. In cylindrical coordinates the boundary conditions are as follows:

$$v_r(0,\theta,0) = v_\theta(0,\theta,0) = 0,$$
$$v_r(0,\theta,H) = v_\theta(0,\theta,H) = 0,$$ (3)
$$v_z(0,\theta,H/2) = 0$$

For small deformations, the nonpenetration condition can be simplified as

$$u_r(D/2,\theta,z) - v_r(d/2,\theta,z) + \Delta R \geq 0 \, ,$$ (4)

where $\Delta R = D/2 - d/2$ is the clearance between the hole and the fastener, and u_r is the radial displacement of the composite plate.

The minimum potential energy principle along with the Lagrangian multiplier method were used to solve the problem. Frictionless contact is considered. The first variation of the following functional is required to vanish.

$$\delta\left(\Pi_p + \Pi_b + \iint_{\Omega(\theta,z)} \lambda(\theta,z)(u_r(D/2,\theta,z) - v_r(d/2,\theta,z) + \Delta R)dS\right) = 0$$ (5)

The potential energy of the laminate is denoted as Π_p, and the potential energy of the elastic fastener as Π_b. $\Omega(\theta,z)$ is the contact zone on which the relationship (4) becomes an equality. The size and location of this zone is unknown initially. Functional (5) suggests a simple interpretation for the Lagrangian multiplier as the value of the radial stress at the contact surface, i.e., $\sigma_{rr}^{(p)}(D/2,\theta,z) = \sigma_{rr}^{(b)}(d/2,\theta,z) = \lambda(\theta,z); (\theta,z) \in \Omega(\theta,z).$

In the following sections, the spline approximation of the functions included in (5) will be constructed.

1.2   Spline Approximation

Curvilinear coordinates ρ and ϕ were introduced to map the plate with a cutout into a region $0 \leq \rho \leq 1$ and $0 \leq \phi \leq 2\pi$. Coordinate lines of this transformation are shown in Figure 1. The transformation is built according to *[10]* so that the coordinate line $\rho=0$ corresponds to the hole edge and $\rho=1$ to the outer rectangular contour of the plate. The radial lines correspond to ϕ=constant. Sets of B-type cubic basis spline functions

$$\left\{ R_i(\rho) \right\}_{i=1}^{m+3}, \; \left\{ \Phi_i(\phi) \right\}_{i=1}^{k+3}, \; \left\{ Z^{(s)}_i(z) \right\}_{i=1}^{n_s+3} \tag{6}$$

along each coordinate were built upon subdivisions $0 = \rho_0 < \rho_1 < ... < \rho_m = 1$, $0 = \phi_0 < \phi_1 < ... < \phi_k = 2\pi$, and $z^{(s-1)} = z_0 < z_1 < ... < z_{n_s} = z^{(s)}$ so that the s-th ply occupies a region $z^{(s-1)} \leq z \leq z^{(s)}$, and n_s is the number of sublayers in each ply. The subdivision of the ρ coordinate is essentially nonuniform. The interval size increases in geometric progression beginning at the hole edge. The region $0 \leq \rho \leq \rho_h$ in which the curvilinear transformation is quasi-cylindrical is subdivided into m_0 intervals, so that $\rho_h = \rho_{m_0}$. The number of intervals of subdivision m, k, and n_s in each direction along with the mesh nonuniformity characteristics, such as m_0 and the consecutive interval ratio, determine the accuracy of the solution and the size of the problem.

The detailed solution procedure, including determination of the contact region, has been described in *[9]*.

1.3   Failure Criteria

Bearing failure can be manifested by a combined effect of all individual failure modes: tensile fiber breakage, micro-buckling, delamination, matrix cracking, and compression/shear cracking. As a noncatastrophic failure mode *[6]*, it can only be adequately described by taking into account the stress redistribution resulting from damage initiation and growth. As a result of the three-dimensional nature of the stress field in the bearing contact region, the modeling of bearing failure represents a challenging task. It has been accomplished so far in simplified two-dimensional models *[7,8]* that neglect delamination and stacking sequence effects. In the present work, a three-dimensional stress analysis was performed instead to evaluate the magnitude of the interlaminar stress components and the effect of stacking sequence on bearing strength. No effect of stress redistribution due to damage was considered.

To put the stress values in perspective, they were compared to the respective ultimate strength. Six dimensionless functions s_i, $i=1,...,6$, were introduced such that

$$s_1 = \begin{cases} \dfrac{\sigma_{11}}{X_T}, & \sigma_{11} > 0 \\[2mm] \dfrac{\sigma_{11}}{X_c}, & \sigma_{11} < 0 \end{cases}, \tag{7}$$

$$s_2 = \begin{cases} \dfrac{\sigma_{22}}{Y_T}, & \sigma_{22} > 0 \\[2mm] \dfrac{\sigma_{22}}{Y_c}, & \sigma_{22} < 0 \end{cases} \qquad s_3 = \begin{cases} \dfrac{\sigma_{33}}{Y_T}, & \sigma_{33} > 0 \\[2mm] \dfrac{\sigma_{33}}{Y_c}, & \sigma_{33} < 0 \end{cases} \tag{8}$$

$$s_4 = \left| \frac{\sigma_{23}}{S} \right| \qquad s_5 = \left| \frac{\sigma_{13}}{S} \right| \qquad s_6 = \left| \frac{\sigma_{12}}{S} \right|. \tag{9}$$

The stress components σ_{ij}, $i, j=1,2,3$ are in ply material coordinates, and the x_1-axis coincides with the fiber direction. Parameters X_T and X_c are the tension and compression strength of

the unidirectional laminate in the fiber direction, Y_T and Y_c are the tension and compression strength in the transverse direction, and S is the in-plane shear strength. The in-plane shear strength is also used for scaling the interlaminar shear stress components.

Bearing loading generates a three-dimensional state of stress in the vicinity of the hole edge. Comparison of the stress components to the respective ultimate material direction strengths neglects mode interaction. In the present work, the use of interactive failure criteria, such as Tsai-Wu *[11]* or Hashin *[12]*, has been avoided because of a lack of experimental evidence supporting the reliability of strength prediction by these criteria in a three-dimensional state of stress as well as under stress gradients. All stress components in the present paper will be examined separately by using Equations (7)-(9).

Three-dimensional ply level analysis performed in the present paper results in stress singularities at the ply interface and the hole edge intersections. In order to predict the onset of failure, a point stress criterion was applied. Failure initiation was predicted when one of the functions s_i, *i=1,…,6,* has an absolute value greater than one at a distance of a ply-group (two plies) thickness away from the hole edge. The choice of a one ply-group thickness characteristic distance was influenced by Kim and Soni *[13]* who used a one-ply thickness characteristic distance with an average stress failure criteria for prediction of delamination onset.

1.4   Numerical Results and Discussion

A schematic of the bearing specimen is shown in Figure 1. To perform the dimensional-dimensional stress analysis and to apply the failure criteria, a full set of thermoelastic and strength characteristics is needed. Because of a lack of sufficient data on the material tested in *[6]*, a similar T300/5250 material was used for the analysis. The

stiffness and strength parameters for T300/5250 are given in Table 2. The estimated

temperature difference between the room temperature and the cure temperature, required for

residual stress calculation, was -100°C. Bearing load was applied through the displacement

boundary conditions (1). The applied bearing stress was calculated as

$$\sigma_B = \frac{1}{AD} \int_0^H \int_0^A \sigma_x(L, y, z) \, dy \, dz \qquad (10)$$

Table 2
Material Properties Used in Modeling

Elastic Constants	Failure Parameter
$E_1 = 181.0$ GPa $E_2 = E_3 = 10.3$ GPa $\nu_{12} = \nu_{13} = 0.28$ $\nu_{23} = 0.40$ $G_{12} = G_{13} = 7.17$ GPa $G_{23} = 3.68$ GPa $\alpha_1 = 0.02 \times 10^{-6}/°C$ $\alpha_2 = 22.5 \times 10^{-6}/°C$	$X_T = 1500$ MPa $X_C = 1500$ MPa $Y_T = 40$ MPa $Y_C = 246$ MPa $S = 68$ MPa

The subdivisions in the circumferential and radial directions in the plate were k=36

and m=18, with m_0=12 intervals in the near hole region and the size ratio q=1.2. The

subdivisions in the radial and circumferential directions in the fastener were k_b=36, m_b=8,

and q_b=1.2. Two sublayers through the thickness of each ply were used. Only the upper half

of the laminate was modeled because of symmetry.

First, the effect of stacking sequence on stress components was examined. The load

level corresponding to failure of the weaker of the two specimens was chosen, so that

σ_B=318MPa. The influence of stacking sequence on the in-plane stress components is

illustrated in Figure 2. The functions s_1, s_2, and s_6, introduced in Equations (7)-(9), are

a)

s$_1$ ----- specimen C: [0$_2$/90$_2$/+45$_2$/-45$_2$]$_s$

s$_1$ ----- specimen N: [0$_2$/+45$_2$/90$_2$/-45$_2$]$_s$

b)

s$_2$ ----- specimen C: [0$_2$/90$_2$/+45$_2$/-45$_2$]$_s$

s$_2$ ----- specimen N: [0$_2$/+45$_2$/90$_2$/-45$_2$]$_s$

c)

s$_6$ ----- specimen C: [0$_2$/90$_2$/+45$_2$/-45$_2$]$_s$

s$_6$ ----- specimen N: [0$_2$/+45$_2$/90$_2$/-45$_2$]$_s$
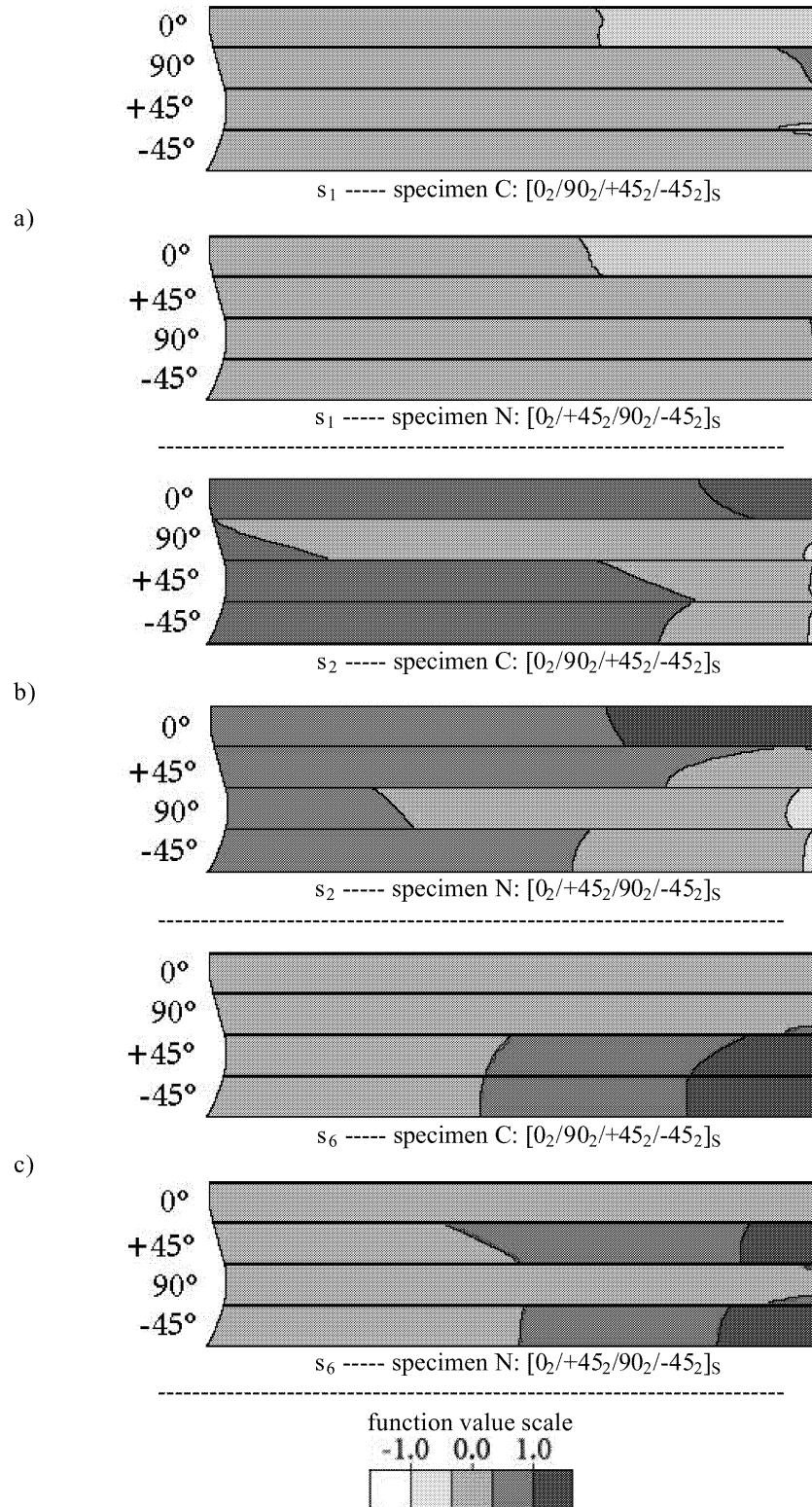
function value scale

-1.0   0.0   1.0

Figure 2. Stacking Sequence Effect on the In-Plane Stress Components at the Bearing Plane for Both Specimens.

shown on the bearing plane. This location was chosen due to available experimental evidence showing the bearing plane to be a critical damage area in the specimens. Both specimens had holes with a relatively small diameter (compared to specimen dimensions) and exhibited bearing-type failure. Five gray-scale color codes are used to display the results. The white regions correspond to $s_i < -1$ (i.e., compression failures), and the darkest regions correspond to $s_i > 1$ (i.e., tensile failures) for $i=1,2,3$. In the case of the shear stresses, the functions s_i, $i=4,5,6$, can only have positive values. The largest effect of the stacking sequence change on in-plane stress components can be seen for the transverse normal stresses. Figure 2b shows that the $s_2 > 1$ region (tensile matrix cracking) in the $0°$ ply is twice as large in specimen N compared with specimen C. This can be explained by the strong reinforcing effect of the $90°$ ply in specimen C compared with the weaker reinforcing effect of the $45°$ ply in specimen N. The fiber direction normal and in-plane shear stresses, Figures 2a and 2c, do not show a significant stacking sequence effect. It should be mentioned that the function values should be compared in the same plies in the two specimens. For example, the difference in appearance of the shear stress function, s_6, in Figure 2c is deceptive. The distribution of s_6 in the $45°$ and $90°$ plies in both specimens is quite similar.

Interlaminar stresses developed at the bearing plane were also examined. Of the three interlaminar components, the transverse shear stress, σ_{13}, was found to extend over the largest region where the ultimate value was exceeded. Figure 3c shows the contour plots of the function s_5 [Equation (9)]. For both specimens, σ_{13} exceeded its ultimate value in the vicinity of the hole edge. In the case of the stronger specimen, C, the area where $s_5 > 1$ is much smaller and consists of two isolated subregions at the 90/45 and 45/-45 interfaces. The other interlaminar shear stress component, σ_{23}, reflected in Figure 3b by function s_4, exhibits
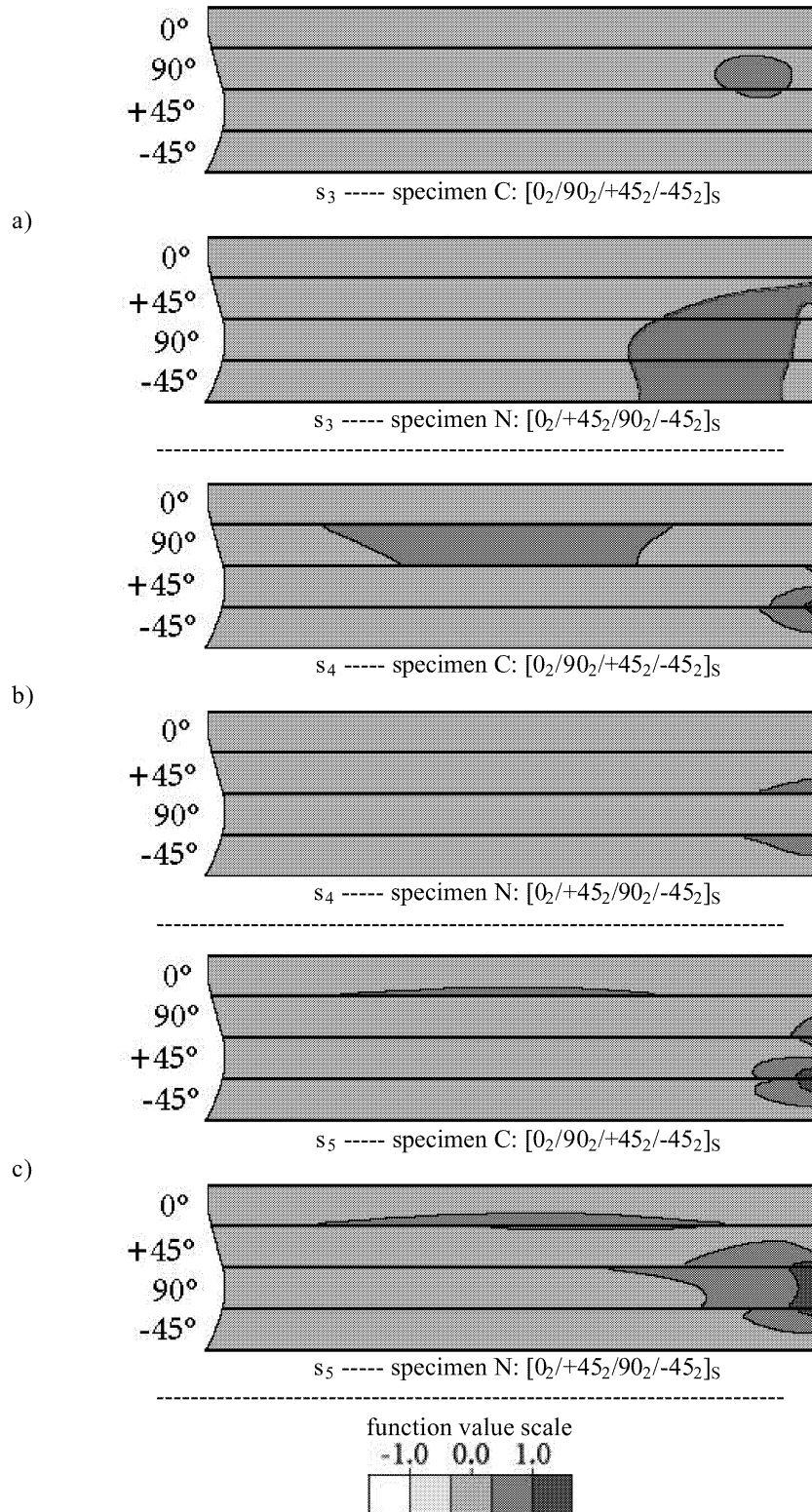
Figure 3. Stacking Sequence Effect on the Interlaminar Stress Components at the Bearing Plane for Both Specimens.

lower values. The function s_3, related to the transverse normal stress, is shown in Figure 3a.

Compared to s_5 it also displays lower values; however, a significant difference in the

distributions between the two laminates can be seen. The weaker laminate, N, displays

significant tensile stresses throughout the laminate thickness, whereas laminate C has

significant transverse normal tensile stress only in a small region in the 90° ply and at the

90/45 interface. This is in qualitative agreement with the cross-sectional micrographic

studies of the failed specimens in Reference *[6]*. The cross section of specimen N shows

significant expansion in the z-direction with open delaminations in addition to transverse

shear-induced 45° matrix cracking and fiber buckling bands. In the case of specimen C, the

failed cross section is significantly less expanded in the transverse direction, with

delamination clearly visible, but with much less opening. It must be noted that the

correlation outlined above is qualitative, because the stress state obtained under the

assumption of a virgin specimen is not valid at the advanced stages of damage.

The x-rays of the two failed specimens, obtained from *[6]*, show different patterns of

0° ply splits. The failure load was σ_B =318 MPa and σ_B =360 MPa for specimen N and

specimen C, respectively. The functions s_2 and s_6 were analyzed at these load levels in the 0°

ply in both specimens near the interface with the underlying ply. The observed matrix

cracking can be produced both by the in-plane transverse tensile stress component and the

in-plane shear stress component. Figure 4 displays superimposed gray-scale plots of the

functions s_2 and s_6. Only two s_i value intervals, $s_i<1$ and $s_i>1$, are shown for each function.

The white area corresponds to $s_i<1$. The light gray corresponds to $s_6>1$, the dark gray to

$s_2>1$, and the medium gray designates the area where both $s_i>1$. Figure 4 also displays the

schematics of the matrix cracks in the 0° plies. They are distributed in a relatively
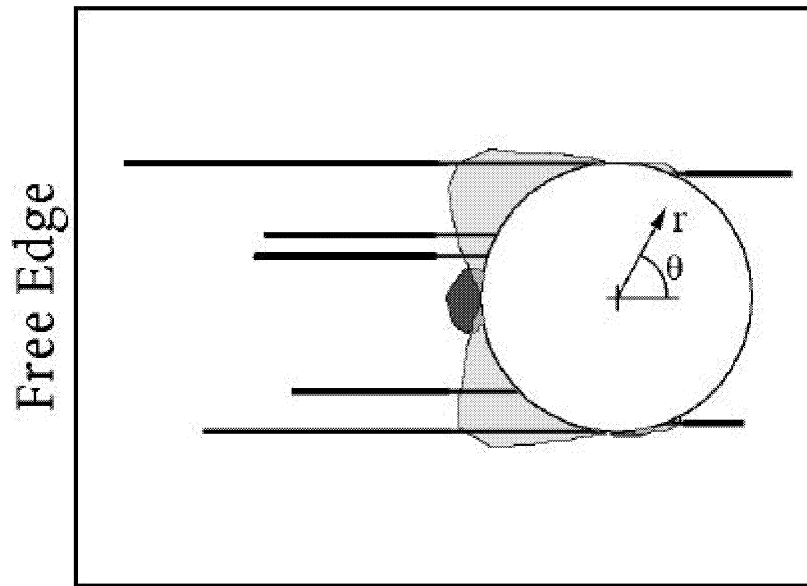
Specimen C: [$0_2/90_2/+45_2/-45_2$]s

Specimen N: [$0_2/+45_2/90_2/-45_2$]s

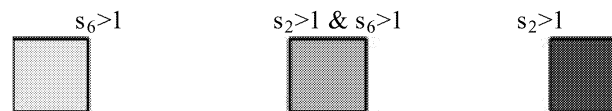$s_6 > 1$ $s_2 > 1$ & $s_6 > 1$ $s_2 > 1$
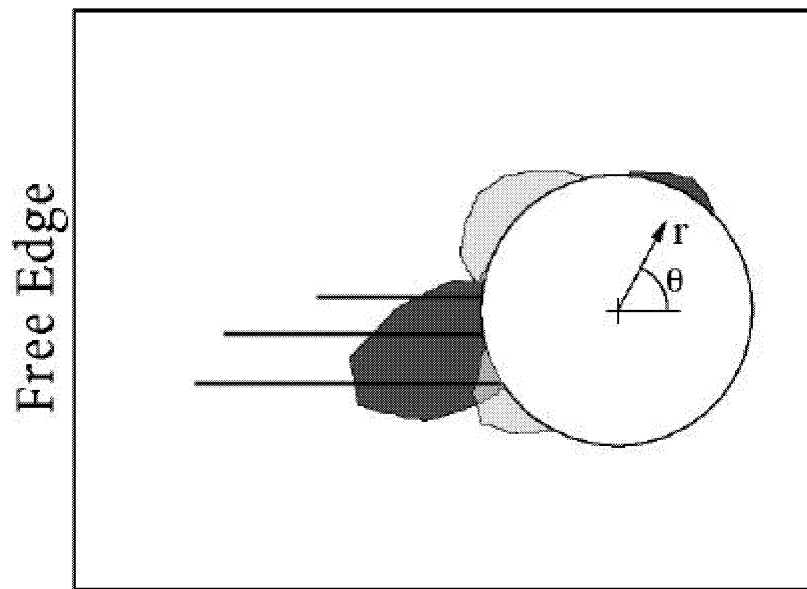
Figure 4.   Comparison of s_2 and s_6 for 0° Plies in Both Specimens at their Respective Failure Loads. The straight solid lines represent the most clearly distinguishable 0° ply cracks obtained from x-rays published in Reference [1].

symmetrical manner in laminate C and in a distinctly nonsymmetrical pattern in laminate N. These crack distributions agree well with distributions of the combined fields of $s_2 > 1$ and $s_6 > 1$ in each laminate displayed in Figure 4. It is worth noting that the application of Hashin's *[12]* matrix cracking criteria, which combines the shear, transverse normal, and interlaminar normal stress components, also provides good agreement with the 0° ply splitting patterns in the two specimens.

Failure initiation prediction was performed by examining criteria (7)-(9) at one ply-group thickness away from the hole edge. The two specimens appeared to have the same initial damage mode – tensile matrix cracking in the 0° and 90° plies. Figure 5 shows the s_2 distribution in these plies at the load levels when the $s_2 > 1$ region reached the dashed contour, which is a double ply thickness (one ply-group) away from the hole edge. This occurred in the 0° ply at 80 MPa and in the 90° ply at 96 MPa in specimen N and in the 0° ply at 128 MPa and in the 90° ply at 112 MPa in specimen C. In the 0° ply this region is in the vicinity of the bearing plane, and in the 90° ply there are two regions at opposite sides of the hole. Interestingly, the cracking of 0° and 90° plies is predicted in reverse order for the two laminates. The tensile transverse stress component is the dominating stress component at these locations.

1.5   Conclusions

1. Three-dimensional stress analysis in quasi-isotropic laminates under bearing loading was performed to explain the effect of stacking sequence on the pin bearing strength observed in *[6]* by calculating accurate stress fields in undamaged plies.

2. A significant effect of stacking sequence was observed on transverse normal in-plane stress component and predicted failure initiation loads. The specimen with the lower

0° Ply at 128 MPa bearing stress on the top face of the laminate

90° ply at 112 MPa bearing stress near the 90/+45 interface

Specimen C: $[0_2/90_2/+45_2/-45_2]_S$

0° Ply at 80 MPa bearing stress on the top face of the laminate

90° ply at 96 MPa bearing stress near the 90/-45 interface

Specimen N: $[0_2/+45_2/90_2/-45_2]_S$

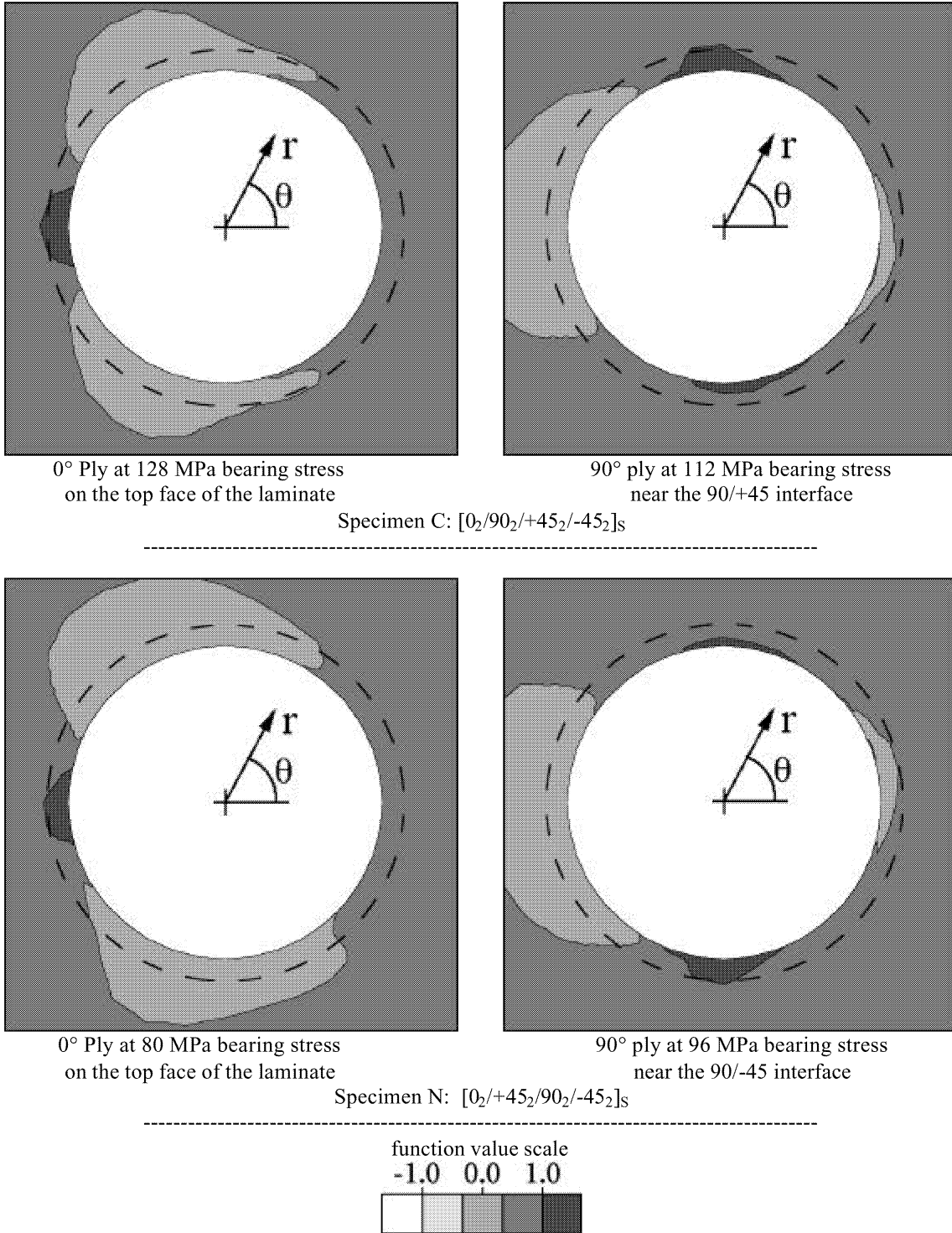function value scale

-1.0   0.0   1.0

Figure 5.   Initial Damage Prediction for Both Specimens (Function s_2). The dashed lines represent a radius equal to the hole radius plus 1 ply-group thickness.

18

bearing strength exhibited lower damage initiation loads and a larger critical transverse normal tensile stress ratio area in plies with the same orientation. The 0° ply cracking patterns observed in experiments agree with superimposed in-plane shear and transverse normal stress maps.

3. Transverse shear and normal stresses were analyzed at the bearing plane of the specimens. A larger area of critical transverse shear stress ratio was found in the specimen with lower bearing strength. The transverse normal stress at the bearing plane of the weaker specimen had large areas of significant tensile values correlating with massive thickness expansion and delamination under bearing loading. The stronger specimen had smaller areas of significant tensile transverse normal stresses through the thickness of the bearing plane, which is consistent with the smaller thickness expansion and mostly compression shear failure pattern observed.

2. PROPERTY DEGRADATION BASED PROGRESSIVE DAMAGE MODELING IN OPEN-HOLE COMPOSITE LAMINATES

To provide accurate strength prediction in notched composites, it is important to take into account the stress redistribution due to damage progression prior to failure. Finite-element formulation and property degradation rules are used through [14-26] to address this issue. Two-dimensional property degradation-based models were developed for strength prediction in open-hole [14-17], pin-loaded [18] and bolted with clamp-up [19-21] composite laminates. The effect of clamp-up in [19-21], which is essentially a three-dimensional effect, was taken into account by introducing a washer-plate friction correction to the bearing load. This allowed estimation of the clamp-up effect within two-dimensional formulations, based on lamination theory. Papers [14-16,18] used essentially similar property degradation models, consisting of Hashin's [12] failure criteria and selected elastic moduli discounts within the element. The thermal residual stresses were neglected. Both linear and nonlinear geometric and constitutive modeling were considered in [18]. Five local failure options were implemented: (i) matrix tensile failure resulting in zero transverse modulus, (ii) matrix compressive failure also resulting in zero transverse modulus, (iii) fiber-matrix shearing failure resulting in zero in-plane shear modulus, (iv) fiber tensile failure resulting in complete stiffness loss of the element, and (v) fiber compression (bearing) failure. Different post-failure property degradation rules were used for this (v) failure mode in the linear and nonlinear analysis models. In the linear analysis the effect of fiber compression failure was the same as fiber tensile failure and resulted in complete loss of element stiffness. On the contrary, in the nonlinear analysis model the failure mode (v) resulted in stiffening the element by increasing all elastic moduli 10 times. The nonlinear

model included geometric nonlinearity and cubic in-plane shear stress-strain relationship with nonlinearity coefficient, which is obtained by best fit of the [±45]s coupon stress-strain curves. It was concluded that the final failure load can be predicted usually to within 20 percent of the experimental results. Inclusion of the nonlinear effects was found to improve the predictions. It is of interest, however, as to how much of that improvement is due to changing the property degradation rule for the fiber compression failure mode in the critical bearing failure region from loss of stiffness to "incompressibility."

A discrete internal state variable approach to property degradation was taken in *[17]*. Two types of damage, matrix failure and fiber breakage, were considered. The stiffness degradation in the lamina did not depend on the cause of the damage. A quadratic, non-interactive fiber failure criterion was applied. Matrix cracking was considered to occur in the element if the Tsai-Wu *[11]* criterion was satisfied, and the fiber failure criterion was not met. The degraded stiffness moduli were represented as

$$E_{11} = D_1 E_{11}^0, \quad E_{22} = D_2 E_{22}^0, \quad G_{12} = D_6 G_{12}^0,$$

Empirical knockdown factors D_1, D_2 and D_6 were used to degrade the stiffness and, as expected, the values of these parameters had a significant effect on final failure prediction. The transverse cracking related factors were constant for all cases $D_6 = D_2 = 0.2$, and the fiber breakage related factor D_1 varied from 0.07 for the AS4/3502 system to 0.001 for the T300/1034-C system. Thermal and moisture effects were incorporated. Interestingly, the residual stresses in all cases resulted in higher predicted strength values. In the damage accumulation studies reported, the model tended to under-predict the fiber breakage initiation loads and over-predict the extent of fiber failure regions. This likely resulted from

difficulties in accurately describing the local fiber stress relaxation, due to transverse splitting and smoothing the drastic effect of stress redistribution due to fiber failure, by considering only 0.001 to 0.07 times knockdown factors, respectively, for this failure mode. These effects can be accurately predicted only by using 3-D modeling methods. With a proper choice of the property degradation factors, the strength of laminates reported in the paper was predicted to within 14 percent.

An internal state, variable-matrix crack density was introduced in *[21]* to modify the nonlinear property degradation models of *[14-16,18]*. Exponential, property degradation rules resulted in more stable numerical mechanisms. It was concluded in *[22]* that the developed method is capable of predicting the strength and failure mode of composite joints under combined bearing and axial bypass loads. It was also noted that to fully account for the factors affecting the strength of composite bolted joints, the analysis needs to be extended to three dimensions.

Recently several three-dimensional progressive damage models were developed for strength prediction in open-hole *[23,24]* and bolt-hole laminates *[25,26]*. Three-dimensional property degradation modeling described in *[23]* was facilitated in an ABAQUS environment and consisted of modified Hill failure criteria described in *[18]* and associated property degradation rules. The following damage modes were incorporated: fiber failure, corresponding to property degradation rule $E_{11}=G_{12}=0$, $v_{13}=v_{12}=0$, matrix in-plane failure, corresponding to $E_{22}=G_{12}=0$, $v_{31}=v_{32}=0$, and matrix failure due to out-of-plane stress components, modeled as $E_{33}=G_{31}= G_{32}=0$, $v_{21}=v_{23}=0$. To model the delamination within the property degradation framework, the authors introduced a resin reach layer with the properties of cured matrix between each ply. Due to computational constraints this layer had

the same thickness as the unidirectional plies. Several examples were considered. Axial

splits in a 0^0 ply emanating from a crack-type notch under axial tension were modeled. Good

agreement of the experimentally observed split length as a function of load was shown.

Symmetric cross-ply laminates with open holes under uniaxial tension were also considered.

It was stated that the strength of the laminate was predicted with five percent accuracy, and

that the presence of the resin reach layer did not significantly affect the prediction.

Evaluation of damage distribution shows qualitative agreement with the radiographic image.

The residual stresses were not accounted for in the analysis.

An internal state variable approach to establish property degradation rules was taken

in *[24,25]*. Two failure mechanisms were incorporated in *[24]*: the matrix transverse

cracking and fiber tensile breakage. The degraded stiffness matrix due to transverse cracking

was represented as

$$C_{ij} = C_{ij}^0 e^{k_{ij}a_f}$$

where C_{ij}^0 was the initial (before damage) stiffness matrix, a_f the damage variable, and k_{ij} the

rates of individual stiffness component degradation, established from the self-consistent

model. Fiber breakage was detected from maximum strain failure criterion. Commercial

finite-element package SAMSEF was chosen to implement the methodology. Numerical

results presented were for the same laminates as in two-dimensional analysis *[17]*. It was

concluded that more realistic transverse cracking patterns in the off-axis plies were observed.

The loading was modeled only up to about 85 percent of the failure, due to numerical

concerns. No residual stress or delamination effects were considered.

The discrete internal state variable approach developed in *[17]* for two-dimensional

analysis was extended in *[25]* for three-dimensional prediction of bearing strength in

composite bolted joints. A rigid bolt was modeled and ABAQUS finite element package was used to facilitate the property degradation model. Hashin's failure criterion [12] was used to identify the damage mode in the element. Two different sets of internal state variables, D_i^t and D_i^c, associated with tensile and compressive loads were used. Linear eight-node elements with reduced integration were utilized for the three-dimensional modeling with one element through the thickness of the ply. The delaminations and residual stresses were neglected. In the bearing failure mode, the analysis was stopped after the damage propagated outside the washer-covered area around the hole. The model proved capable of predicting the mode of failure: tensile, shear-out or bearing, and the initial load drop-off. No detailed correlation of the damage progression prediction was made with the experiment.

A complex boundary condition contact problem of transverse bending of a composite plate with a countersunk bolt was considered in [26]. Complete element failure approach was adopted for property degradation modeling. In this model the element stiffness was completely degraded if any one of the incorporated failure criteria was met for the average stress component values of the element. In [26] the maximum stress failure criterion was used for in-plane damage and Ye [27] delamination failure criterion for damage caused by out-of-plane stresses. Thus through the complete element failure approach, the delaminations were included in the model. No residual stresses were considered. The model was shown to produce load deflection curves in good agreement with the experimental results for the $[90_8/0_8]_s$ and $[0_8/90_8]_s$ laminates. However, no detailed correlation of the damage progression prediction was made with the experiment.

Both two- and three-dimensional models have been developed for strength prediction of composites with open and filled holes. The property degradation methodologies used for

three-dimensional analysis were direct extensions of the ones developed for two-dimensional analysis. The multi-scale nature of the failure process in composites requires certain assumptions to be made in order to formulate the property degradation algorithm. The empirical constants entering the analysis provide tuning mechanisms in order to achieve accurate strength prediction for a given material system within a certain range of parameters. This was demonstrated in numerous two-dimensional studies reviewed above. Note that only one method *[17]* takes into account the residual stresses in the laminates. Three-dimensional progressive damage analysis alleviates one level, namely, the through-the-thickness of the laminate, level of averaging in the stress analysis. The price for that is at least an order of magnitude increase in computer time and resources for an entry-level practical laminate, e.g. an eight-ply quasi-isotropic symmetric laminate. The redemption for this treatment should be no less than a physically meaningful and verified damage origination and progression sequence prediction, in different types of laminates such as soft and 0^0 dominated laminates made of material systems with different toughness.

In the present report a three-dimensional property degradation algorithm will be implemented to account for the residual stress and delamination effects. The focus of the study will be on investigating the mesh type and density effect aspects of modeling which are specifically important in three-dimensional property degradation-based damage initiation and progression modeling.

2.1   Problem Formulation

Consider a rectangular *N*-layer laminate built of orthotropic layers with length *L* in the x-direction, width *A* in the y-direction, and thickness *H*. Individual ply thicknesses are $h_p = z^{(p)} - z^{(p-1)}$, where $z = z^{(p)}$ and $z = z^{(p-1)}$ are upper and lower surfaces of the p-th ply,

respectively. The origin of the *x,y,z* coordinate system is in the lower left corner of the plate, as shown in Figure 1. A circular opening of diameter *D* with the center at x=x_c and *y*=y_c is considered. Uniaxial loading is applied via displacement boundary conditions at the lateral sides (x=0,L), while all other boundaries were kept free:

$$-u_x(0,y,z) = u_x(L,y,z) = u_L/2,$$
$$u_y(0,y,z) = u_y(L,y,z) = 0,$$

(11)

The transverse displacement is not constrained aside from a rigid body constant. The constitutive relations in each ply are as follows:

$$\sigma_{ij} = C_{ijkl}^p(\varepsilon_{kl} - \alpha_{kl}^p \Delta T)$$

(12)

where C_{ijkl}^p and α_{kl}^p are elastic moduli and thermal expansion coefficients of the p-th orthotropic ply, and ΔT is the temperature change.

2.2   Variational Considerations

Consider volume V and sub-volume V_1, which for correctness may be considered surrounding a crack (Figure 6). We shall impose a number of stress conditions to be satisfied within V_1:

$$F_m(\sigma_{ij}) = 0, \ m = 1,2,... \ .$$

(13)

The Reissner-Hellinger variational principle

$$R = \iiint\limits_V (\sigma_{ij}(\varepsilon_{ij} - \frac{1}{2}(u_{i,j} + u_{j,i})) + U(\varepsilon_{ij}))dV - \iint\limits_{S_t} T_i u_i ds,$$

where T_i are applied external tractions, will be considered here and below summation upon repeated indexes is implied. The Lagrangian multiplier method is used to impose additional conditions (13):
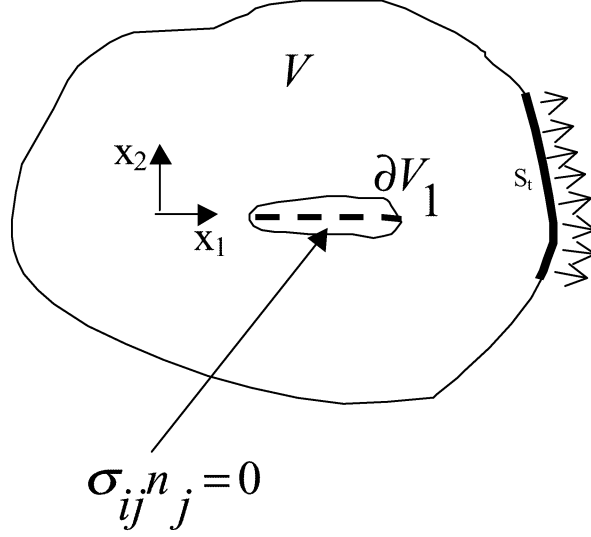
26

Figure 6. Additional Stress Conditions Applied in the Subvolume V_1.

$$\delta\left[R + \sum_m \iiint_{V_1} \lambda_m F_m(\sigma_{ij}) dV \right] = 0 \qquad (14)$$

The independent variations of (14) yield:

$$\delta u: \ \sigma_{ij,j} = 0, x \in V, \sigma_{ij} n_j = T_i, x \in S_t$$

$$\delta\varepsilon: \ \frac{\partial U}{\partial \varepsilon_{ij}} = \sigma_{ij} \qquad (15)$$

$$\delta\sigma: \begin{cases} \varepsilon_{ij} = u_{(i,j)}, x \in V/V_1 \\ \varepsilon_{ij} = u_{(i,j)} + \sum_m \lambda_m \frac{\partial F_m}{\partial \sigma_{ij}}, x \in V_1 \end{cases} \qquad (16)$$

where

$$u_{(i,j)} = \frac{1}{2}(u_{i,j} + u_{j,i})$$

As follows from Equation (15), the additional stress conditions (13) are contributing to displacement strain relationship in the sub-volume V_1. For some practically meaningful cases, the Lagrangian multipliers can be explicitly obtained. Let

$$F_m = \sigma_{qm}, m = 1,2,3$$

For $q=2$ it corresponds to a crack in the plane $x_2=0$, as shown in Figure 6. Substituting Equation (15) into the second equation (16), one will obtain the following relationship within volume V_1

$$\sigma_{ij} = C_{ijkl}(u_{(k,l)} - e_{kl} - \delta_{qk}\lambda_l), \quad e_{kl} = \alpha_{kl}\Delta T \tag{17}$$

where δ_{qk} is Kronechker's delta. First assume that only one component of stress $\sigma_{qp} = 0$, then, according to Equation (17)

$$\lambda = \frac{C_{qpkl}(u_{(k,l)} - e_{kl})}{C_{qpqp}},$$

where summation is carried out only upon k and l. Substituting this equation back in (17) one obtains

$$\sigma_{ij} = C^*_{ijkl}(u_{(k,l)} - e_{kl}), \tag{18}$$

and

$$C^*_{ijkl} = C_{ijkl} - \frac{C_{ijqp}C_{qpkl}}{C_{qpqp}}. \tag{19}$$

It follows from equation (19) that the degraded stiffness matrix C^*_{ijkl} is a symmetric matrix with zeroes in the row and column qp. In order to satisfy all three conditions, $\sigma_{qj} = 0$, j=1,2,3, the degradation operator (19) can be applied recursively. It can be shown that the final degraded stiffness matrix is independent of the order in which (19) is applied. Similar results can be obtained intuitively by degrading Young's moduli E_2 and G_{12} with additional and less intuitive considerations regarding Poisson's ratio coefficients.

2.3   Progressive Damage Modeling

In all further analyses the ply material axes are oriented as follows: x_1 is the fiber direction, and the x_3 axis is directed perpendicular to the lamina plane. Three types of damage will be implemented in the analysis: (i) fiber breakage ($\sigma_{1j} = 0$, j=1,2,3), (ii) in-plane transverse cracking ($\sigma_{2j} = 0$, j=1,2,3), and (iii) interlaminar transverse cracking ($\sigma_{3j} = 0$, j=1,2,3). A combination of these damage types is modeled by requiring the combined set of stress components to be zero. Maximum stress failure criterion was utilized to sample each element at the center. Nine coefficients were computed:

1.   Fiber direction tension failure : $f_1 = \max(0, \dfrac{\sigma_{11}}{X_t})$

2.   Fiber direction compressio n failure : $f_2 = -\min(0, \dfrac{\sigma_{11}}{X_c})$

3.   In - plane tensile transvers e cracking : $f_3 = \max(0, \dfrac{\sigma_{22}}{Y_t})$

4.   In - plane compressiv e transvers e cracking : $f_4 = -\min(0, \dfrac{\sigma_{22}}{Y_c})$

5.   Interlamin ar tensile cracking : $f_5 = \max(0, \dfrac{\sigma_{33}}{Y_t})$

6.   Interlamin ar compressiv e cracking : $f_6 = -\min(0, \dfrac{\sigma_{33}}{Y_c})$

7.   Transverse shear matrix cracking : $f_7 = \left| \dfrac{\sigma_{23}}{S_t} \right|$

8.   Transverse shear matrix cracking : $f_8 = \left| \dfrac{\sigma_{13}}{S_t} \right|$

9.   Shear in - plane matrix cracking : $f_9 = \left| \dfrac{\sigma_{12}}{S} \right|$

Coefficients f_i are always positive and $f_i =1$ indicates local failure mode. Criteria 1 and 2 indicate failure breakage and lead to conditions (i); criteria 3, 4 and 9 indicate in-plane

transverse cracking and lead to conditions (ii); criteria 4-8 indicate interlaminar failure and are modeled by applying stress conditions (iii).

Progressive damage modeling is performed by incrementing the damage rather then the load. Each step of this procedure calculates the load increment required to introduce additional damage. In case of linear constitutive law, the first load increment obtained through this scheme corresponds to damage initiation. To take into account the residual stress, two boundary condition problems with different boundary conditions are solved at each step. One of them is the mechanical uniaxial loading (11) under unit load with zero thermal stresses, and the other is the thermal loading with all free-edge (less rigid body motion) boundary conditions, corresponding to residual stresses. The flow-chart of the progressive damage analysis algorithm is as follows:

1. Input and zero damaged elements.

2. Solve the mechanical loading problem (11) at $u_L=0.001L$ for $\Delta T=0$ and determine f_i^M in each element.

3. Solve the thermal loading problem for given ΔT under all free-edge boundary conditions and determine f_i^T in each element.

4. Calculate loading coefficient $P = \min_{\substack{J \\ all\,elements}} \dfrac{1-f_j^T}{f_j^M}$ and record the element and mode for which it was calculated.

5. Determine damage mode (I), (ii), (iii) from the previous step. Degrade the properties by consecutively applying degradation operator (19).

6. Go to step 2.

The procedure is implemented in computer code SVELT1.2 allowing for various types of displacement approximation basis functions.

2.4   Numerical Results

Numerical results and experimental data were obtained for a material system IM7/5250-4 by using the set of elastic properties described in Table 3. In all cases linear displacement approximation, corresponding to eight-node brick elements, was used, with the exception of the geometry models. In the present work exact curvilinear transformations were used as opposed to isoparametric elements. The strength properties in fiber and transverse directions were obtained by testing unidirectional eight-ply thick laminates and the shear properties by testing [45/-45]$_{4s}$ laminates. All specimens were 7" wide and 2" long. The notched specimens had either a 0.25-inch or 0.5-inch central hole. Unnotched quasi-isotropic [45/0/-45/90]$_s$ coupons were analyzed first. The predicted and experimental stress-strain curves are shown in Figure 7. The beginning of the numerical curve corresponds to failure initiation and correlates well with experimental values. The analysis predicts that the failure initiation load is very close to the 90° ply failure load [all elements fail in mode (ii)]. At approximately 0.77 percent strain, a stiffness loss is predicted which is due to transverse cracking of the ±45 plies. The ultimate strain is controlled by fiber failure and is the same for experiment and prediction. The significant strength underprediction is essentially due to overprediction of the stiffness degradation in the ±45 plies. The over-softening effect of the present analysis is due to complete stiffness degradation in the transverse direction due to transverse cracking (ii). The remedy in this case will be limiting the transverse stiffness degradation by lower limit values due to saturation of the transverse cracking density *[29,30]*.

31

Table 3
Material and Strength Properties Used in Modeling

```
1   material type (1-elastic orthotr.) [psi]
E11=2.215E+07    Xt=3.497E+05    Xc=3.031E+05
E22=1.300E+06    Yt=9.610E+03    Yc=4.139E+04
E33=1.300E+06
U13=3.270E-01
U23=4.770E-01
U12=3.270E-01
G13=8.670E+05
G23=4.770E+05
G12=8.670E+05    S=1.451E+04    S13=1.251E+04
A11=2.500E-07
A22=1.400E-05
Stress free temperature T=350⁰F
```
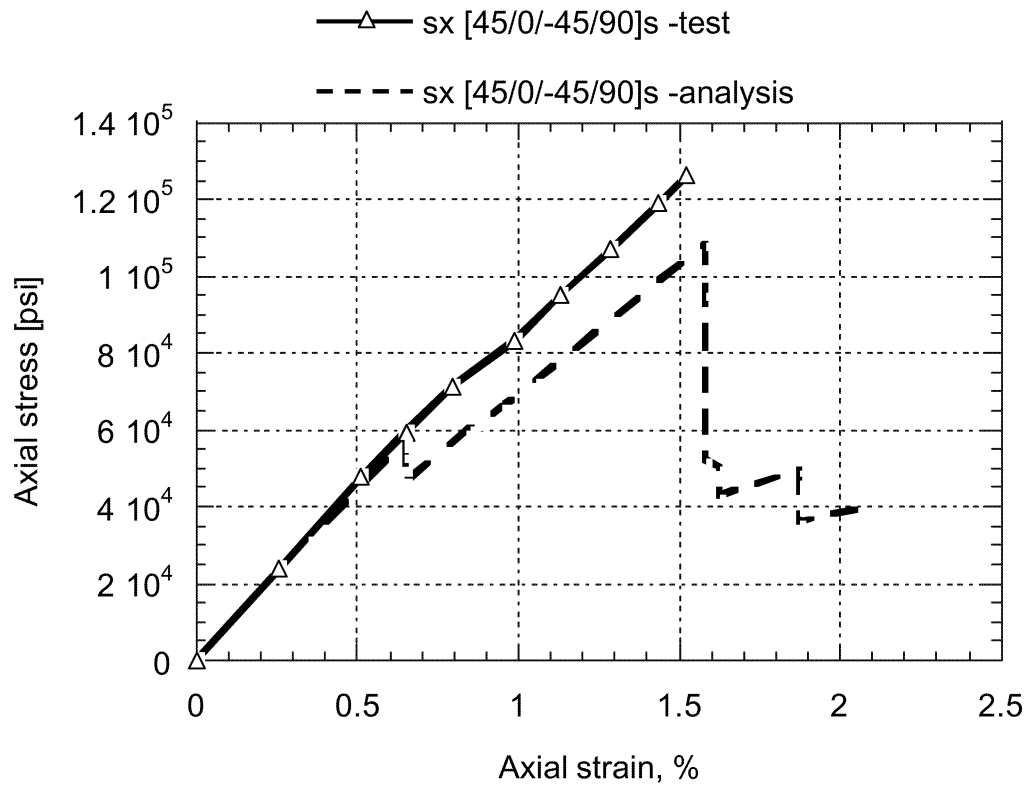

Figure 7. Experimental and Predicted Stress-Strain Curves of a [45/0/-45/90]s Laminate.

Three-dimensional damage propagation modeling in notched laminates imposes severe requirements on the capability of the finite-element modeling. Namely, it is natural to expect that a three-dimensional finite-element model, which is successful in predicting the strength of the laminate, should be able to predict the strength of each of its plies. Thus the strength prediction in the $[0_8]$ laminate is considered next. The experimentally observed failure mode of this laminate is development of transverse cracks or splits emanating from the hole which reduce the stress concentration in the fiber direction, and provide the strength of the laminate equal to that of the ligament strength. This mechanism will be present in the laminate, where the splits may not propagate through the entire length of the laminate and will only provide partial stress concentration relief. Typical finite-element subdivision, shown in Figure 8, will be utilized. The progressive failure analysis, however, predicts early onset of fiber breakage due to inability to model the stress relief in the fiber direction. To illustrate this fact the following numerical examples were considered. In the finite-element mesh shown in Figures 8a and 8b, all the elements with the center coordinates x_i, y_i, z_i, such that $y_c - D/2 < y_i < y_c + D/2$, were assigned to have in-plane matrix cracking-type damage (ii). This band of elements is darkened in Figure 8. The mesh size is chosen sufficiently small, so that the roughness of the edges of this band near the hole is much smaller than the hole diameter. The radial distribution of the hoop stress σ_{xx}/σ_0 normalized to applied far-field stress is shown in Figure 9. The two mesh densities yield practically equal hoop distribution for virgin laminates. In the presence of massive transverse damage, however, the hoop stress is reduced very little. Significant relief of the stress concentration can only be observed if the stiffness of the selected finite elements is completely reduced, i.e. (i)+(ii) degradation conditions applied. This assumption is physically incorrect since no massive fiber breakage
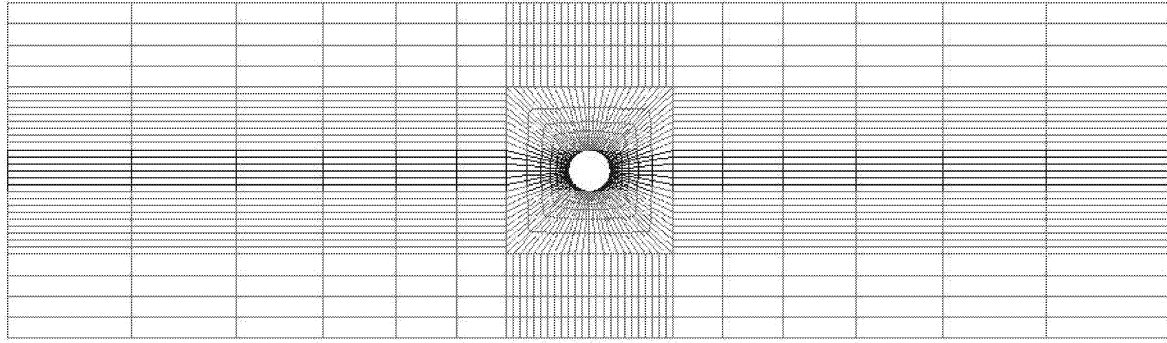
(a)
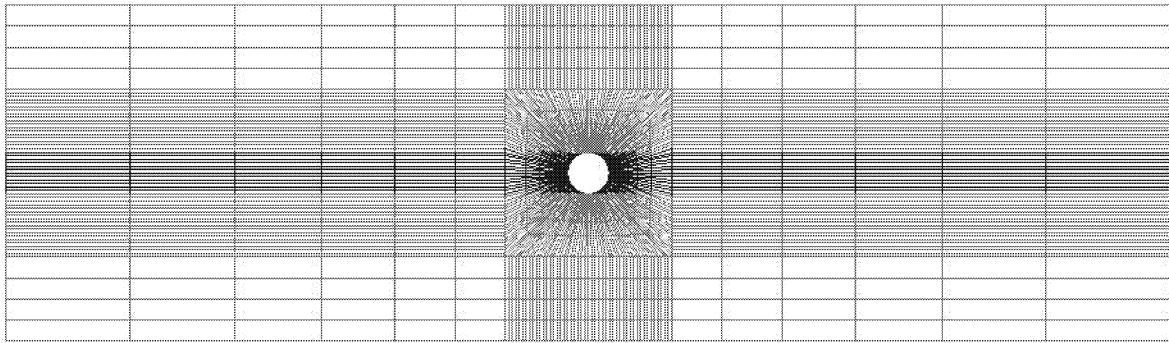
(b)

Figure 8. Radial Type Mesh Configurations Used for Predicting the Fiber Stress Relaxation due to Transverse Splitting: (a) Coarse Mesh; (b) Dense Mesh.
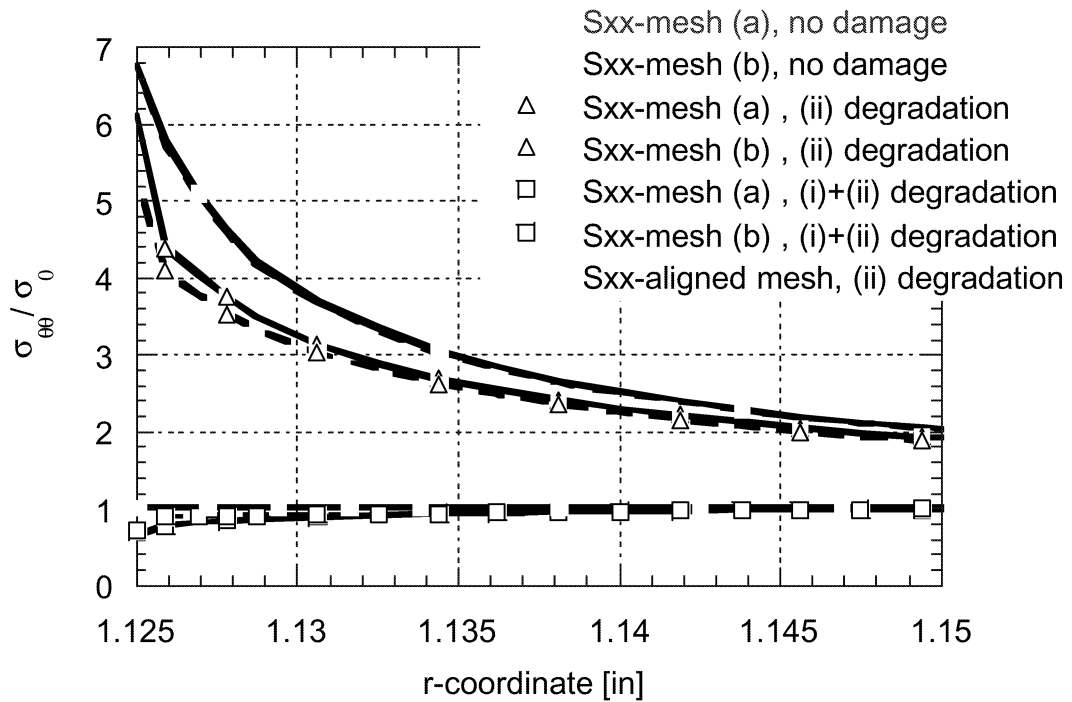

Figure 9. Normalized Hoop Stress $\sigma_{\theta\theta}/\sigma_0$ Distribution as a Function of the Distance from the Hole Edge in the Direction Perpendicular to Loading.

in the selected regions is observed. The effect, pointed out above, appears to be finite-element mesh type dependent. A different type of mesh, with the element edges aligned with the damage propagation direction, was used next for analysis. The mesh is shown in Figure 10. Similar tests conducted with this mesh showed that by applying the transverse cracking-type property degradation to the elements within the selected band, one observes a complete relaxation of the hoop stress, as shown in Figure 9. Progressive damage modeling performed with this mesh for unidirectional laminates with two hole sizes is shown in Figure 11. The experimentally-obtained strength value for the 0.25-inch-diameter hole is 307 ksi and is very close to the prediction.

The new mesh type does not represent a solution to the mesh type dependent behavior of damage propagation and stress redistribution. There are no reasons to expect that the mesh shown in Figure 10 will be more suitable for progressive damage analysis in off-axis plies than the radial mesh. It illustrates, however, the additional difficulties in three-dimensional property degradation modeling which were not addressed in previous works *[23-26]*.

2.5   Conclusions

A 3-D progressive damage analysis method has been developed. Nine maximum stress failure criteria have been used for local failure prediction. Residual stresses have been included into the analysis.

Damage propagation modeling in notched specimens shows significant dependence upon mesh type and density.

Accurate transverse cracking prediction (including thickness effect) has a significant influence on final failure prediction of both notched and unnotched specimens.
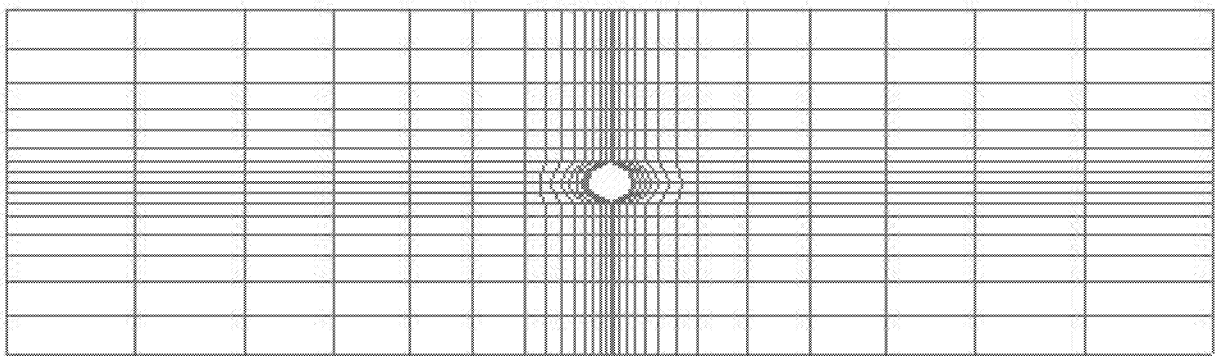
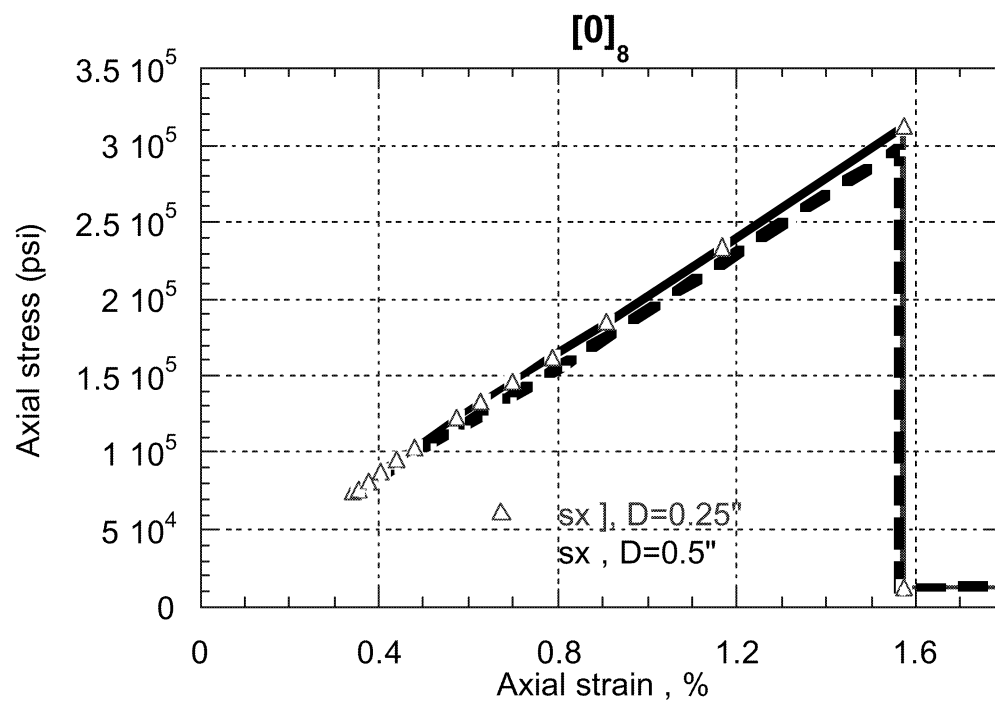**Figure 10. Configuration of the Mesh with the Element Edges Aligned with the Damage Propagation Directions.**

Figure 11. Predicted Stress-Strain Curves for the [0]₈ Laminate with Different Hole Sizes.

3. DAMAGE INITIATION AND PROGRESSION IN MULTIDIRECTIONAL LAMINATES WITH A HOLE

3.1   Experiment

A series of tension tests were conducted to document the initiation and propagation of damage in multidirectional composite laminates with a centrally located circular hole. Testing was also conducted for unnotched tensile coupons to determine the first-ply failure and ultimate strength to compare with the hole specimens. The hole specimens were tested under a series of incremental loadings to document the initiation and progression of damage and the corresponding strain response. Acoustic emission data were also collected during loading and compared to strain measurements and radiographic images to identify significant damage events. Additional analysis was conducted by comparing experimental strain data to results obtained from elasticity theory and from spline variational theory.

The material system chosen for this work is graphite/toughened bismaleimide, IM7/5250-4. Two types of laminates, $[0_2/90_2]_s$ and $[\pm30/90_2]_s$, were considered. The thermoelastic properties necessary for analysis were determined from testing of $[0]_{8T}$, $[90]_{8T}$ and $[\pm45]_{2s}$. Each laminate was cured according to the manufacturer's recommended cure cycle and was postcured at 440°F for a duration of five hours and 40 minutes. The average fiber volume was found to be 62 percent, and the void content was determined to be less than one percent.

In multidirectional laminates, the holes were drilled using a carbide-tipped steel drill bit with an operating speed of 800 rpm based on an optimization study to minimize drilling-induced damage. Prior to initial loading, a radiographic inspection of each specimen